

THE K2 M67 STUDY: REVISITING OLD FRIENDS WITH K2 REVEALS OSCILLATING RED GIANTS IN THE OPEN CLUSTER M67

DENNIS STELLO^{1,2,3}, ANDREW VANDERBURG⁴, LUCA CASAGRANDE⁵, RON GILLILAND⁶, VICTOR SILVA AGUIRRE³, ERIC SANDQUIST⁷, EMILY LEINER⁸, ROBERT MATHIEU⁸, DAVID R. SODERBLOM⁹

Draft version October 25, 2021

ABSTRACT

Observations of stellar clusters have had a tremendous impact in forming our understanding of stellar evolution. The open cluster M67 has a particularly important role as a calibration benchmark for stellar evolution theory due to its near solar composition and age. As a result, it has been observed extensively, including attempts to detect solar-like oscillations in its main sequence and red giant stars. However, any asteroseismic inference has so far remained elusive due to the difficulty in measuring these extremely low amplitude oscillations. Here we report the first unambiguous detection of solar-like oscillations in the red giants of M67. We use data from the *Kepler* ecliptic mission, K2, to measure the global asteroseismic properties. We find a model-independent seismic-informed distance of 816 ± 11 pc, or $(m - M)_0 = 9.57 \pm 0.03$ mag, an average red-giant mass of $1.36 \pm 0.01 M_{\odot}$, in agreement with the dynamical mass from an eclipsing binary near the cluster turn-off, and ages of individual stars compatible with isochrone fitting. We see no evidence of strong mass loss on the red giant branch. We also determine seismic $\log g$ of all the cluster giants with a typical precision of ~ 0.01 dex. Our results generally show good agreement with independent methods and support the use of seismic scaling relations to determine global properties of red giant stars with near solar metallicity. We further illustrate that the data are of such high quality, that future work on individual mode frequencies should be possible, which would extend the scope of seismic analysis of this cluster.

Subject headings: stars: fundamental parameters — stars: oscillations — stars: interiors — techniques: photometric — open clusters and associations: individual (M67)

1. INTRODUCTION

M67 is an open cluster with approximately solar age and metallicity, making it a prime target in stellar astrophysics for decades. After the demonstrated success of applying seismic techniques to the Sun (e.g. Duvall et al. 1984; Christensen-Dalsgaard et al. 1985), recent decades also saw studies aimed to detect solar-like oscillations in these cluster stars, mainly around the main sequence and the turn-off (Gilliland et al. 1991, 1993). However, success was limited, due to the extremely low amplitude oscillations. In the hope of obtaining unambiguous detections a 6-week 10-telescope multi-site campaign was launched, aimed to detect oscillations in the cluster’s giant stars (Stello et al. 2006, 2007). With only marginal detections at best, this campaign concluded the past two decades of ground-based attempts. Fortunately, the *Kepler* space telescope turned out to be an incredible source of asteroseismic data, clearly showing oscillations in open cluster red giants. This allowed inferences to be made on cluster age, mass loss along the giant branch, and seismic member-

ship (e.g. Stello et al. 2010; Basu et al. 2011; Miglio et al. 2012; Stello et al. 2011b); including results showing that the oscillation amplitudes anticipated for the giants by previous ground-based campaigns were generally overestimated (Stello et al. 2011a). With *Kepler*’s ecliptic second-life mission, K2 (Howell et al. 2014), its potential for seismic studies of open clusters increased because of the many clusters within its new viewing zone. In particular, data from its observing campaign 5 has been much anticipated because it included M67.

In this paper, we report the first results in a series arising from a large collaboration aimed at observing and studying M67 using K2 time series photometry. After a description of our general target selection, we focus on the analysis of the red giant cluster members. Initially we make comparisons with previous attempts to detect oscillations, and follow on with measuring the global asteroseismic properties from which we determine stellar radius, mass, and age. We compare these results with independent literature values and investigate the asteroseismic scaling relations, widely used for radius and mass estimation.

2. OBSERVATIONS AND LIGHT CURVE PREPARATION

The goal of the general target selection for the K2 M67 study was to include all stars for which extensive kinematic information (Geller et al. 2015) supports even a modest probability of cluster membership. Sample completeness in the majority of the cluster has been assured by using a 400 by 400 pixel (26.5’ by 26.5’ square)¹⁰ superaperture centered on the cluster, which is recorded and downloaded to ground in its entirety. Outside the dedicated aperture, all known or

¹⁰ The superaperture size corresponds to approximately six core radii of the cluster (see Geller et al. 2015, and references therein)

¹ Sydney Institute for Astronomy (SIFA), School of Physics, University of Sydney, NSW 2006, Australia

² School of Physics, University of New South Wales, NSW 2052, Australia

³ Stellar Astrophysics Centre, Department of Physics and Astronomy, Aarhus University, DK-8000 Aarhus C, Denmark

⁴ Harvard-Smithsonian Center for Astrophysics, Cambridge, MA 02138, USA

⁵ Research School of Astronomy & Astrophysics, Mount Stromlo Observatory, The Australian National University, ACT 2611, Australia

⁶ Department of Astronomy and Astrophysics, The Pennsylvania State University, University Park, PA 16802, USA

⁷ San Diego State University, Department of Astronomy, San Diego, CA 92182, USA

⁸ Department of Astronomy, University of Wisconsin-Madison, Madison, Wisconsin 53706, USA

⁹ Space Telescope Science Institute, Baltimore, Maryland 21218, USA

suspected cluster members were added as single targets; we adopted $\langle P_{RV}, P_{PM} \rangle > 20\%$ to be inclusive. The superaperture and all added targets for M67 were observed for about 75 days (Campaign 5, 27 April - 10 July, 2015) in the spacecraft’s long-cadence mode (29.4 min), while a few were also observed in short cadence (58.85 sec). Extensive cross-checks verified that all the giant members were included in our proposal (e.g. all Stello et al. 2006 targets).

For this investigation, the extraction of photometric time series (light curves) was performed using the technique by Vanderburg & Johnson (2014) with the updates described in Vanderburg et al. (2016) both for single targets and those captured by the superaperture. For some of the giants, we processed the light curves in a slightly different manner. The Vanderburg & Johnson (2014) method accounts for low-frequency variations in K2 light curves by modeling them with a basis-spline, usually with breakpoints every 1.5 days. For giants with oscillation frequencies around $\sim 10 \mu\text{Hz}$, we used a faster spline with breakpoints every 0.3 days to model the low-frequency variations, which in these cases are dominated by the seismic oscillations. Modeling the oscillations with a faster spline decreased the noise level in the light curves. Of the resulting light curves, about 70% arose from the superaperture.

The post processing of the data follows that described in Stello et al. (2015). In short, we apply a high-pass filter and fill short gaps, using linear interpolation. The applied filter had a characteristic cut-off frequency of $\sim 3 \mu\text{Hz}$ for most stars, and $\sim 6 \mu\text{Hz}$ for the low-luminosity red giant branch (RGB) stars ($V > 12.4$). The light curves of the two most luminous stars were not high-pass filtered, to avoid affecting the oscillation signal.

3. STELLAR SAMPLE AND COMPARISON WITH PREVIOUS RESULTS

For the following asteroseismic analysis, we selected all giant stars with available K2 data if they were listed as kinematic members by Geller et al. (2015) and were following the giant branch including the helium-burning phase in the Hertzsprung-Russell diagram (Figure 1). This seismic sample is unique in the way it spans the entire RGB, bottom-to-tip, and the helium-core burning ‘red clump’ (RC) phase of a simple stellar population. Whether it includes any asymptotic giant branch stars is unknown. However, generally stars brighter than the RC but fainter than the RGB tip are most likely RGB stars. We do note that while EPIC211409660 and 211407537 have effective temperatures compatible with the isochrone RGB they have luminosities near the asymptotic giant branch luminosity bump (Salaris & Cassisi 2005), located at $V \sim 9.6 - 9.7$. We calculated the power density frequency spectra for all the giants, to reveal the presence of oscillations. The color-magnitude diagram shows all giant members showing oscillations (Figure 1, black dots with open circles).

The power spectra of a representative sample of our giant targets are shown in Figure 2 (black curves) with ordinate and abscissa ranges identical for all stars. The panels are ordered by brightness, indicative of relative luminosity for cluster stars, going from brightest at top left to faintest at bottom right. It is unambiguous that we see oscillations for the entire range of evolutionary stages spanned by the cluster giants. The figure illustrates nicely how amplitude and timescale of both the granulation (downward sloping background noise) and of the oscillations (hump indicated by arrows) scale with luminosity (Kjeldsen & Bedding 2011; Stello et al. 2011a; Mathur et al. 2011; Kallinger et al. 2014). It is also evident

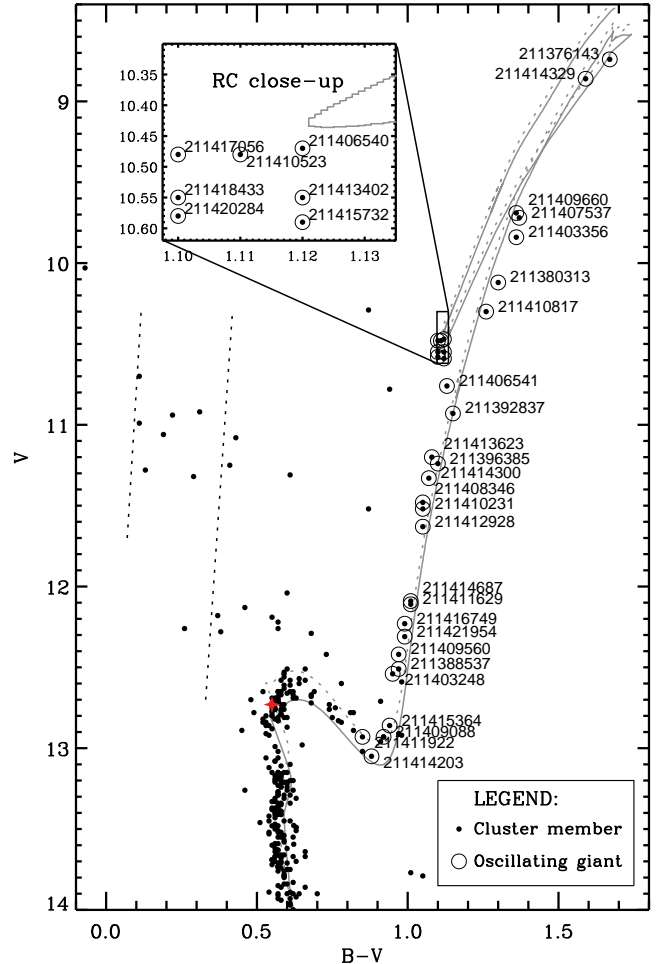


FIG. 1.— Color-magnitude diagram of M67 cluster members. Photometry (not corrected for reddening) is from Montgomery et al. (1993) and membership is from Geller et al. (2015). Stars with detected oscillations are circled and indicated by their EPIC-ID. Gray curves show BaSTI isochrones of 3.5 Gyr (dotted) and 4.0 Gyr (solid) (Pietrinferni et al. 2004), shifted 9.7 mag vertically and 0.03 mag horizontally. The instability strip is shown by dotted black lines (Rodríguez & Breger 2001). The eclipsing binary HV Cnc is marked by a red star symbol.

at high frequencies that the largely photon-dominated (white) noise increases towards fainter stars.

Our clear detection of oscillations naturally leads to the question of whether previous ground-based campaigns did indeed detect this signal. For this, we focus on Stello et al. (2007) who specifically targeted the giants. In Figure 2 we show stars in common with Stello et al. (2007) (gray). We conclude that the reported excess power by Stello et al. (2007) could quite plausibly be oscillations for the most luminous stars in their sample, near the red clump luminosity, while it seems unlikely oscillations were detected for the lower luminosity RGB stars. A similar comparison with the one giant (211408346), which fell serendipitously in the turn-off star sample studied by Gilliland et al. (1993), showed noise levels 5-10 times too high in the ground-based data to plausibly see evidence of the oscillations.

4. EXTRACTING SEISMIC OBSERVABLES

To demonstrate that we can perform meaningful seismic analyzes including extracting the large frequency separation, $\Delta\nu$, and the frequency of maximum power, ν_{max} (and in

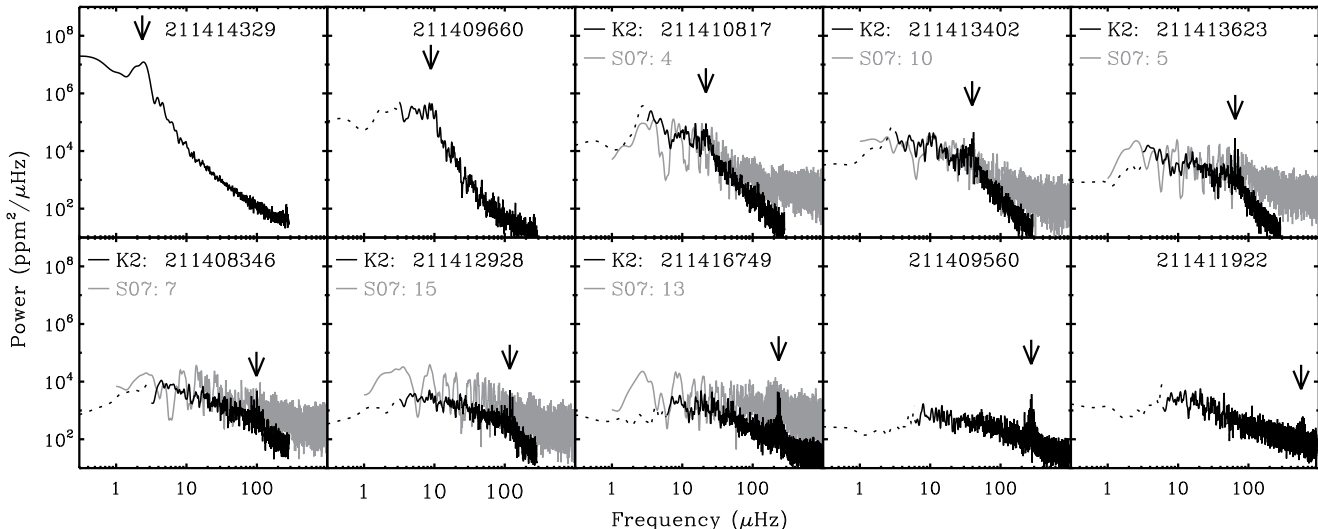


FIG. 2.— Power spectra from K2 data of 10 representative giants (black). The region affected by high-pass filtering is indicated (dotted curve). Ground-based results (Stello et al. 2007, S07) are also shown (gray). The K2 and ground-based spectra are smoothed to a common frequency resolution. Arrows indicate the oscillation power. Both EPIC and S07 IDs are shown.

many cases possibly individual frequencies), we show regions of power spectra and échelle diagrams centered around ν_{\max} in Figure 3. For stars with $\nu_{\max} \lesssim 10 \mu\text{Hz}$, we expect the uncertainty in $\Delta\nu$ to be relatively large, limited by the frequency resolution of the K2 data (Stello et al. 2015). For the most luminous star (top) we therefore over plot a comparison spectrum in red of a similar star observed for four years by *Kepler*. With a formal frequency resolution of $\sim 0.15 \mu\text{Hz}$ from the K2 data we only obtain the broad features of the underlying mode structure, ‘just’ enough to measure $\Delta\nu$, which also explains the somewhat blurry échelle diagram for this star. Comparing the échelle diagrams from top (near the RGB tip) to bottom (near RGB bottom) we see the known gradual increase in the location of the radial mode ridge (see vertical dotted lines), also known as the offset, ε , in the asymptotic relation for acoustic oscillations as observed by e.g. Huber et al. (2010); Mosser et al. (2011); Corsaro et al. (2012). For the star in the bottom panel we start to see the slight decrease in ε , as expected from models (White et al. 2011).

Using the method by Huber et al. (2009) to analyze the power spectra, we were able to detect $\Delta\nu$, ν_{\max} , and oscillation amplitude for all the observed giants of M67, except four stars near the bottom of the RGB, which were only observed in the spacecraft’s long-cadence mode. Non-detections among these stars are expected because they oscillate beyond the long-cadence Nyquist (half the sampling) frequency of $\sim 283 \mu\text{Hz}$, making it harder to measure the seismic signal. We were, however, able to measure the signal for another two such ‘super-Nyquist’ stars (see Yu et al. 2016, for a similar technique applied to field giants). In addition, the super-Nyquist issue was mitigated for four giants, for which K2 short-cadence data were also available. Despite that, the star sitting at the very bottom of the RGB (211414203), showed only marginal detection due to the intrinsically lower oscillation amplitude and increasing photon noise towards less evolved and fainter stars. Also, the largest and most luminous giant in our sample (211376143) oscillates at such low frequency that $\Delta\nu$ cannot be measured. We list our measured ν_{\max} and $\Delta\nu$ values in Table 1 (columns 4-5), and plot them together with oscillation amplitude in Figure 4a. It is evident

that the stars with small error bars line up almost perfectly on a straight line in $\Delta\nu$ - ν_{\max} space as expected for stars with almost the same mass (e.g. Stello et al. 2009; Huber et al. 2010). The isochrone in Figure 4a (gray) has a mass-change along the RGB of less than $0.03M_{\odot}$. Significant differences in mass move stars above or below a straight line in this diagram (e.g. Stello et al. 2009; Hekker et al. 2011). This demonstrates that these stars are excellent candidates for testing the seismic scaling relations for different evolution stages where most properties are otherwise similar for all the stars. To further support the detection of oscillations, we show that the amplitude- ν_{\max} trend follows that of solar-like oscillations in field red giants (Figure 4a; lower inset). We were not able to obtain robust measurements of oscillation amplitude for the two most luminous stars.

5. BENCHMARKING SEISMIC SCALING RELATIONS AND MASS LOSS

Having several giants in various evolution stages enables us to estimate the stellar masses along the RGB and RC, and in combination with eclipsing binaries, to benchmark the seismic scaling relations (Jeffries et al. 2013; Sandquist et al. 2013; Brogaard et al. 2012). In addition, one can look for evidence of mass loss (Miglio et al. 2012). To do this we first need T_{eff} for as many stars as possible.

5.1. Temperature scales

We used two sources for T_{eff} . Our main source came from applying the Infrared Flux Method (IRFM) methodology by Casagrande et al. (2010) on 31 stars in our seismic sample for which optical (Tycho2 and/or APASS) plus 2MASS photometry was available. Here we assumed $[\text{Fe}/\text{H}] = 0$, $E(B - V) = 0.03$ (e.g. Casagrande & VandenBerg 2014, and references therein), and seismic $\log g$ obtained from ν_{\max} and an initial T_{eff} . The method is only mildly dependent on the adopted gravity and metallicity, and convergence in T_{eff} was reached after one iteration with seismic gravities. The adopted T_{eff} and uncertainties were derived by averaging the results obtained by implementing the aforementioned photometric systems into the IRFM following Casagrande et al.

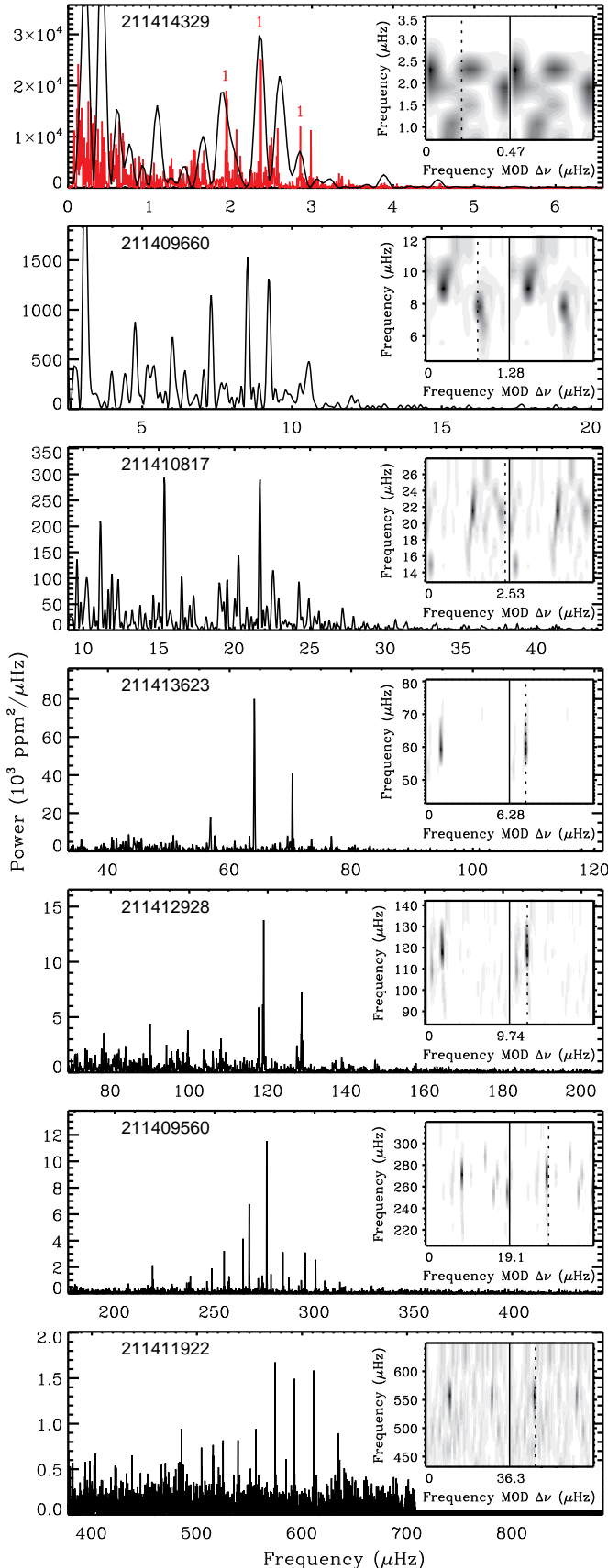


FIG. 3.— Power spectra and échelle diagrams (insets) of seven giants (also shown in Figure 2). The top panel also shows (red) a star observed by *Kepler* with its dipole modes indicated following Stello et al. (2014). The échelle diagrams stack consecutive $\Delta\nu$ -wide bins of the spectrum and are plotted twice side-by-side, as indicated by the black vertical line. The vertical dotted line indicates the approximate location of the radial mode ridge.

(2014). The scatter was used to estimate the uncertainties after increasing it by 20 K to account for the systematic uncertainty on our T_{eff} zero-point (Table 1 column 6). For comparison we also adopted spectroscopically-determined T_{eff} values from SDSS-DR12 (Alam et al. 2015, FPARAM), for the 27-star subset for which T_{eff} was available from both sources (Figure 4b).

5.2. Seismic radius, mass, and age

First, we use the (uncorrected) asteroseismic scaling relations, $\Delta\nu \propto M^{0.5}/R^{1.5}$ and $\nu_{\text{max}} \propto M/(R^2 T_{\text{eff}}^{0.5})$ to determine radius, mass, and $\log g$ for each star (Table 1, columns 7-9). Because the $\Delta\nu$ -scaling is known to show a temperature and metallicity-dependent bias based on stellar models (White et al. 2011; Miglio et al. 2013; Sharma et al. 2016; Guggenberger et al. 2016) we apply the required correction using the public correction software by Sharma et al. (2016, corresponding to option 3 in their Table 1)¹¹; this has been shown to bring seismic masses (and radii) in better agreement with independent determinations from eclipsing binaries and interferometry (compare option 1 and 3 of Table 1 in Sharma et al. 2016, for an overview). The re-derived (corrected) scaling relation-based radii and masses are listed in Table 1 (columns 10-11). We investigate T_{eff} -related systematics by adopting the SDSS-DR12 T_{eff} values, which on average are 90 K hotter than our main IRFM-based values. This shifts the radius ($\sim 1\%$), mass (2-3%), and $\log g$ (~ 0.003 dex) to larger values, of all scaling relation-based results.

In order to also obtain ages we need to apply stellar models, which also provide more precise, but model-dependent, determinations of radius, mass, and $\log g$. For this we use the Bayesian STellar Algorithm (BASTA, Silva Aguirre et al. 2015) with a grid of BaSTI isochrones that includes both RGB and RC models (Pietrinferni et al. 2004). To avoid biases arising from the $\Delta\nu$ -scaling we correct the $\Delta\nu$ values in our BaSTI models applying the prescription of Serenelli (in preparation), which is based on computed oscillation frequencies (analogous to the approach by Sharma et al. (2016)). For each star we adopt the average composition from Pace et al. (2008) ($[\text{Fe}/\text{H}] = 0.03 \pm 0.04$ dex). The results are listed in Table 1 (columns 12-15) and we show the mass and age as a function of ν_{max} in Figure 5. Here the T_{eff} -related systematics are negligible compared to the quoted uncertainties except for a slightly lower SDSS-DR12-based age ($\lesssim 0.08$ Gyr). To highlight metallicity-related systematics we repeat the grid-modelling with $[\text{Fe}/\text{H}] = 0.08 \pm 0.03$ dex (the average from SDSS-DR12), which also show negligible shifts, even for age (+0.03 Gyr).

5.3. Average cluster properties

In the following we present weighted average cluster properties and uncertainties on their mean, and accounting for the systematics described above. To calculate cluster averages we ignore the results from star 211414203 because it is a marginal detection, and 211406541 because its evolutionary state is ambiguous; it appears as an RGB star in the CMD but as an RC star in a $\log g_{\text{seismic}}-T_{\text{eff}}$ diagram (Figure 4b). There is an indication in the power spectrum that the ν_{max} measurement could be underestimated, which we believe is the most likely cause of its deviant mass, and hence age (Ta-

¹¹ Further details about, and access to, the $\Delta\nu$ -correction source code and grid can be found at <http://www.physics.usyd.edu.au/k2gap/Asfgrid/>

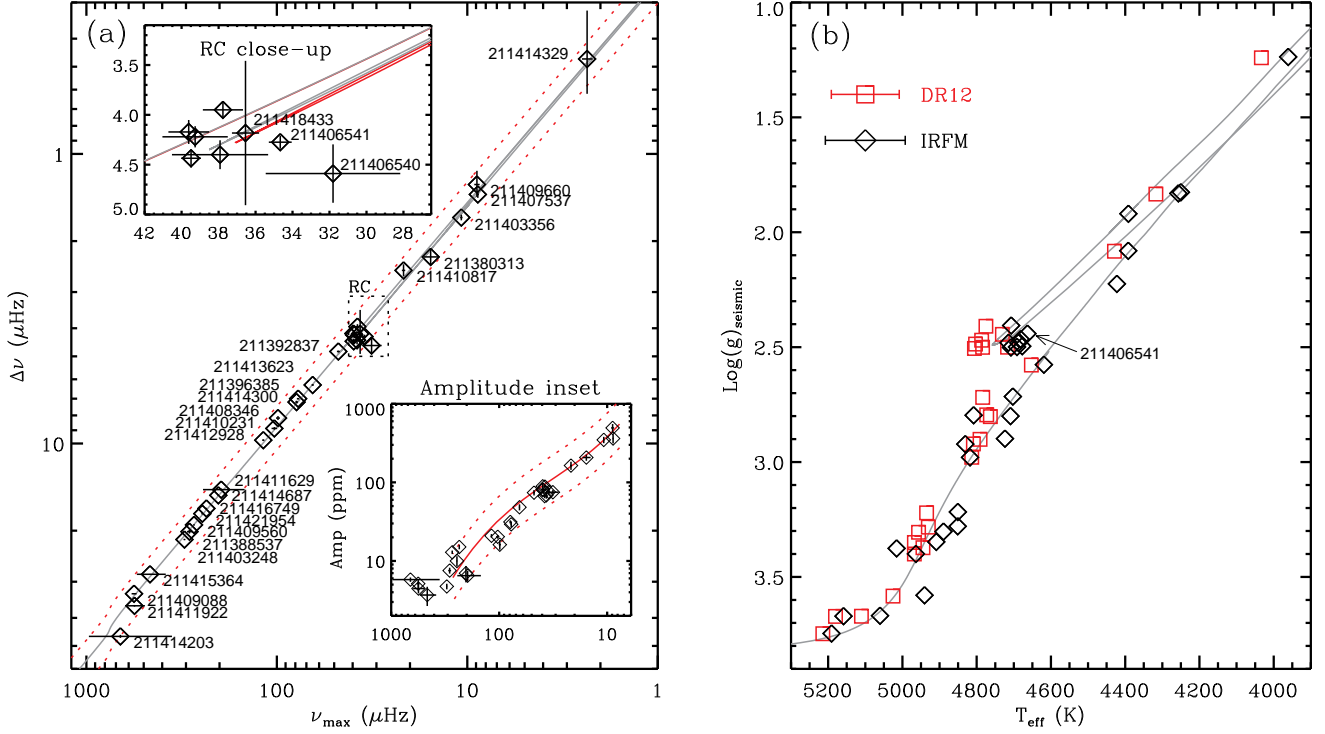


FIG. 4.— (a): Observed $\Delta\nu$ versus ν_{\max} . The solid isochrone from Figure 1 is shown (gray), where ν_{\max} and $\Delta\nu$ are derived using the scaling relations corrected with the Sharma et al. (2016) prescription for $\Delta\nu$. The red dotted curves show typical extremes of the spread for a large sample of giants analyzed the same way as the M67 giants (Stello et al. in prep), and correspond to an uncorrected scaling mass range of 0.75-2.9 M_{\odot} (upper-to-lower curves). EPIC IDs are shown for reference. 1σ error bars are mostly much smaller than the symbols. The RC close-up also shows the isochrone with mass loss of $\eta = 0.2$ (red). In the lower inset the abscissa is replaced by oscillation amplitude per radial mode in parts per million. The red curve shows the average (solid) trend and typical extremes (dotted) from the K2 campaign-1 data. (b) $\log g_{\text{seismic}}-T_{\text{eff}}$ diagram showing all IRFM- (this paper) and SDSS-DR12-based T_{eff} values. Average 1σ error bars are shown.

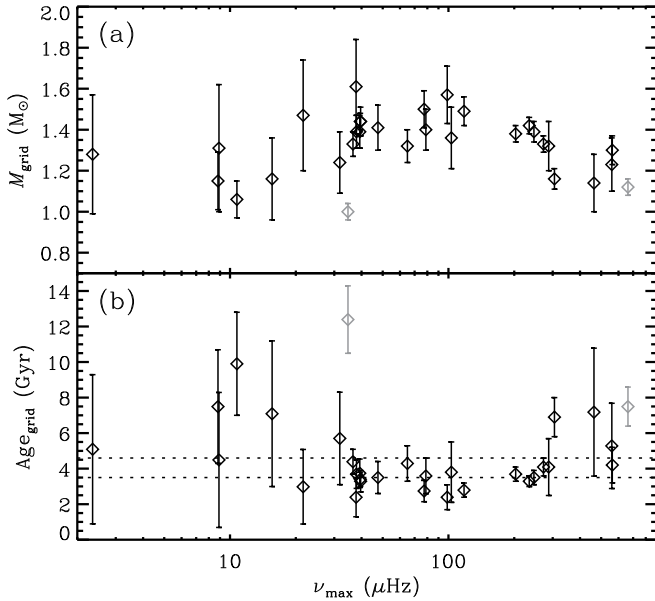


FIG. 5.— (a): M_{grid} versus ν_{\max} including 1σ errorbars. Gray symbols show stars not included in the calculations of the cluster’s average properties (Section 5.3). (b): As (a) but for Age_{grid} . Horizontal dotted lines bracket the typical cluster-averaged age range quoted in the literature (Table 2).

ble 1). We note that 211406540 appears marginally discrepant (Figure 4a, RC close-up), but do not exclude it.

From the seismically-determined radii, we calculate the cluster’s distance modulus, $(m - M)_0$, to be 9.61 ± 0.03 mag (830 ± 11 pc), 9.57 ± 0.03 mag (816 ± 11 pc), and 9.55 ± 0.03 mag (811 ± 11 pc) based on R_{sc} , R_{corr} , and R_{grid} , respectively (Table 1). From R_{corr} we see good agreement between the distances based on RGB (9.57 ± 0.03 mag), and RC (9.59 ± 0.07 mag) stars. Bolometric corrections were performed using the calibrations of Bessell & Wood (1984) and Flower (1996), taking $\sigma(T_{\text{eff}})$ into account, and we assumed $A_V = 3.1E(B - V)$ and neglected the uncertainty in apparent magnitude. In comparison, literature values fall typically in the range 9.5-9.7 mag (795-870 pc) (see Geller et al. 2015, and references therein). Adopting SDSS-DR12 T_{eff} values increases our distance by 0.10 mag (35 pc), while changing $[\text{Fe}/\text{H}]$ has a negligible effect. Changing reddening by 0.01 (Taylor 2007) will change distance by 0.03 mag.

We find the average seismic mass of stars below the RGB bump to be $M_{\text{sc}} = 1.39 \pm 0.02 M_{\odot}$, $M_{\text{corr}} = 1.34 \pm 0.02 M_{\odot}$, and $M_{\text{grid}} = 1.36 \pm 0.02 M_{\odot}$. These are all in agreement with the expected lower-RGB mass, which we derive by extrapolating the dynamic mass, $M_{\text{EB}} = 1.31 \pm 0.05 M_{\odot}$ (Gökay et al. 2013), of the eclipsing binary HV Cnc/S986/WOCS4007 (Sanders 1977; Geller et al. 2015) located near the cluster turn-off ($V = 12.73$, $B - V = 0.55$; Figure 1). To extrapolate, we add the mass difference between the location of the eclipsing binary and that of the RGB along the BaSTI isochrone, which is 0.05-0.09 M_{\odot} for the RGB below the bump, hence resulting in expected masses of about 1.36-1.40 M_{\odot} . Because the uncertainty of the expected mass

TABLE 1
SEISMIC PROPERTIES OF M67 RED GIANTS. SUBSCRIPTS ‘SC’, ‘CORR’, AND ‘GRID’ INDICATE THE SEISMIC METHODS, SCALING, CORRECTED SCALING, AND GRID-BASED MODELLING, RESPECTIVELY.

EPIC ID [1] ^a	WOCS ID [2] ^b	Class [3] ^c	ν_{\max} (μHz) [4]	$\Delta\nu$ (μHz) [5]	T_{eff}/K (IRFM) [6]	R_{sc} (R_{\odot}) [7]	M_{sc} (M_{\odot}) [8]	$\log g_{\text{sc}}$ (cgs) [9]	R_{corr} (R_{\odot}) [10]	M_{corr} (M_{\odot}) [11]	R_{grid} (R_{\odot}) [12]	M_{grid} (M_{\odot}) [13]	$\log g_{\text{grid}}$ (cgs) [14]	Age _{grid} (Gyr) [15]
211376143	1075	SM	0.81(10)											
211414329	1036	SM	2.35(15)	0.47(15)	3960(92)	52.0(3.4)	1.7(2.2)	1.237(32)	50.3(3.3)	1.6(2.0)	44.7(5.0)	1.25(28)	1.235(28)	5.3(4.2)
211407537	1008	SM	8.81(11)	1.38(4)	4250(126)	23.43(45)	1.34(17)	1.826(49)	22.02(43)	1.19(15)	21.7(1.3)	1.15(14)	1.825(6)	7.2(3.2)
211409660	1005	BM	8.90(29)	1.28(13)	4256(116)	27.73(98)	1.90(81)	1.831(45)	26.58(94)	1.75(73)	23.0(2.5)	1.30(29)	1.828(14)	4.6(4.0)
211403356	1045	SM	10.75(15)	1.66(4)	4391(97)	20.12(36)	1.23(13)	1.920(40)	18.85(34)	1.08(11)	18.80(74)	1.06(9)	1.915(7)	9.6(3.0)
211380313	1065	SM	15.6(1.3)	2.27(15)	4391(78)	15.6(1.4)	1.07(40)	2.081(36)	14.5(1.3)	0.93(34)	15.9(1.2)	1.14(19)	2.095(28)	7.5(4.1)
211410817	2004	SM	21.62(44)	2.53(12)	4422(92)	17.53(40)	1.88(38)	2.225(40)	16.73(38)	1.71(34)	15.4(1.4)	1.45(27)	2.224(9)	3.1(2.1)
*211406540	1029	SM	31.8(3.6)	4.59(29)	4707(107)	8.05(93)	0.60(26)	2.406(61)	8.14(94)	0.62(26)	10.98(25)	1.23(15)	2.441(38)	5.7(2.7)
211406541	2014	BM	34.66(62)	4.27(7)	4663(68)	10.07(19)	1.02(9)	2.441(35)	9.62(19)	0.93(8)	9.88(19)	0.99(4)	2.444(6)	12.3(1.8)
*211418433	1022	SM	36.54(74)	4.18(72)	4681(73)	11.11(24)	1.31(91)	2.465(38)	11.16(24)	1.33(92)	11.12(22)	1.33(6)	2.466(9)	4.4(7)
*211410523	1003	SM	37.8(1.1)	3.95(8)	4714(117)	12.92(40)	1.84(23)	2.481(62)	13.02(41)	1.87(23)	12.31(73)	1.63(23)	2.468(15)	2.3(1.1)
*211415732	1009	SM	37.9(2.6)	4.40(14)	4687(110)	10.42(73)	1.20(30)	2.481(59)	10.46(73)	1.21(30)	11.09(16)	1.39(8)	2.487(20)	3.7(8)
*211420284	2019	SM	39.3(1.8)	4.22(11)	4677(89)	11.72(54)	1.57(27)	2.496(46)	11.80(54)	1.59(27)	11.17(21)	1.39(8)	2.482(15)	3.7(8)
*211413402	2005	SM	39.49(54)	4.44(9)	4691(153)	10.68(23)	1.31(14)	2.499(79)	10.73(23)	1.33(14)	11.10(13)	1.43(4)	2.503(6)	3.3(4)
*211417056	2010	SM	39.6(1.1)	4.17(12)	4707(113)	12.14(37)	1.70(25)	2.501(59)	12.23(37)	1.73(25)	11.23(24)	1.43(7)	2.493(11)	3.3(6)
211392837	3042	SM	47.54(86)	4.81(3)	4618(70)	10.85(21)	1.62(10)	2.576(35)	10.33(20)	1.47(9)	10.20(28)	1.42(11)	2.571(9)	3.3(9)
211413623	4005	SM	64.84(83)	6.28(3)	4702(143)	8.77(17)	1.46(9)	2.715(74)	8.39(17)	1.33(8)	8.40(17)	1.33(8)	2.714(7)	4.2(9)
211396385	1033	BM	77.4(1.2)	7.00(4)	4808(290)	8.50(29)	1.65(17)	2.80(16)	8.23(28)	1.55(16)	8.16(17)	1.50(9)	2.792(8)	2.7(6)
211414300	1011	SM	78.8(1.3)	7.19(8)	4709(69)	8.12(15)	1.52(10)	2.800(36)	7.78(14)	1.39(10)	7.79(23)	1.40(10)	2.798(7)	3.5(9)
211408346	2006	SM	98.7(2.3)	8.17(13)	4723(132)	7.90(22)	1.80(19)	2.898(70)	7.59(21)	1.66(17)	7.42(28)	1.57(14)	2.892(10)	2.3(7)
211410231	3011	SM	103.1(3.5)	8.87(9)	4830(147)	7.08(26)	1.53(18)	2.922(86)	6.87(26)	1.44(17)	6.75(29)	1.36(16)	2.914(14)	3.7(1.7)
211412928	4010	SM	117.8(1.5)	9.74(5)	4817(149)	6.70(13)	1.57(10)	2.979(85)	6.50(13)	1.47(9)	6.55(11)	1.49(7)	2.979(6)	2.7(5)
211411629	3004	BM	196(48)	14.43(13)										
211414687	5010	SM	203.0(1.5)	15.10(6)	4850(73)	4.82(5)	1.40(5)	3.217(43)	4.70(5)	1.33(5)	4.77(5)	1.38(4)	3.220(3)	3.6(4)
211416749	4011	SM	234.3(1.3)	16.76(5)	4851(80)	4.51(5)	1.41(5)	3.280(48)	4.40(4)	1.34(4)	4.50(5)	1.42(4)	3.282(3)	3.2(3)
211421954	3019	SM	246.1(2.3)	17.47(6)	4889(78)	4.38(5)	1.41(6)	3.303(48)	4.29(5)	1.35(5)	4.35(6)	1.39(5)	3.303(5)	3.4(5)
211409560	4009	SM	272.2(1.7)	19.10(7)	4908(111)	4.06(5)	1.34(6)	3.347(70)	4.00(5)	1.30(5)	4.05(4)	1.34(4)	3.348(3)	3.9(4)
211388537	2052	SM	287.6(8.7)	20.15(30)	5015(71)	3.90(12)	1.32(15)	3.376(52)	3.91(12)	1.33(15)	3.88(15)	1.31(12)	3.375(12)	4.2(1.5)
211403248	2035	SM	305.5(3.0)	21.45(9)	4963(80)	3.64(5)	1.21(5)	3.400(54)	3.64(5)	1.21(5)	3.57(6)	1.17(5)	3.398(5)	6.5(1.1)
211415364	5014	SM	463(80)	28.29(8)	4940(122)	3.16(55)	1.39(72)	3.58(12)	3.13(54)	1.35(71)	2.95(13)	1.13(14)	3.550(16)	7.4(3.6)
211411922	3017	SM	559(66)	36.34(24)	5158(117)	2.36(28)	0.96(34)	3.67(12)	2.44(29)	1.02(37)	2.57(10)	1.20(13)	3.699(15)	5.6(2.6)
211409088	6012	SM	562(17)	33.02(11)	5060(64)	2.85(9)	1.38(13)	3.669(51)	2.87(9)	1.40(13)	2.79(6)	1.29(7)	3.655(8)	4.3(1.0)
**211414203	10006	SM	663(308)	46.35(55)	5190(77)	1.73(80)	0.61(85)	3.75(31)	1.79(83)	0.65(91)	2.12(4)	1.10(5)	3.821(7)	7.9(1.3)

Uncertainties are shown in compact bracket form: e.g. $2.35(5) = 2.35 \pm 0.05$, $2.35(15) = 2.35 \pm 0.15$, $1.297(32) = 1.297 \pm 0.032$, $15.6(1.3) = 15.6 \pm 1.3$.

^aSee Huber et al. (2016). (sorted by ν_{\max}).

^bSee Geller et al. (2015); includes cross ID to Sanders (1977).

^cClassification and membership from radial velocity (Geller et al. 2015); SM: single member; BM: binary member.

*Red clump star according to CMD.

**Marginal detection.

is at least $0.05M_{\odot}$ (from $\sigma(M_{\text{EB}})$, which is probably underestimated), we are not able to make strong conclusions on which seismic method provides the most accurate mass.

The average RC star mass is $M_{\text{sc}} = 1.37 \pm 0.09 M_{\odot}$, $M_{\text{corr}} = 1.40 \pm 0.09 M_{\odot}$, and $M_{\text{grid}} = 1.40 \pm 0.03 M_{\odot}$, which for the latter two is $0.04\text{--}0.06M_{\odot}$ more massive than for the lower RGB. The RC- RGB mass difference is expected to be only $0.02\text{--}0.05M_{\odot}$, assuming no mass loss along the isochrone. Hence, we see no evidence of significant mass loss along the RGB. This seems to align with the seismic-based results of Miglio et al. (2012) who concluded no or little mass loss (equivalent to Reimers η below 0.2) for the open clusters NGC 6819 and NGC 6791, which bracket the age of M67.

Finally, we obtain an average age of $\text{Age}_{\text{grid}} = 3.46 \pm 0.13$ Gyr for our giants. This is on the lower side compared to traditional isochrone fitting results ranging $3.6\text{--}4.6$ Gyr

(VandenBerg & Stetson 2004), $3.5\text{--}4.0$ Gyr (Sarajedini et al. 2009), chromospheric activity-based ages $3.8\text{--}4.3$ Gyr (Barnes et al. 2016), and recent K2-based gyrochronology results of 3.7 ± 0.3 Gyr (Gonzalez 2016) and 4.2 ± 0.2 Gyr (Barnes et al. 2016), but individual star ages are statistically compatible with those from other methods (Table 1, Figure 5b). We note that the small uncertainty in the adopted average metallicity tends to favor a grid-modeling solution in a single metallicity value, potentially biasing our result. Also, model-dependent age systematics are not taken into account, making our uncertainties underestimated. We would caution adopting this age given the poor match of the 3.5 Gyr isochrone at the turn off in Figure 1, which we attribute partly to uncertainties in the convective core overshoot (Dinescu et al. 1995), and partly to the lack of stronger age constraints from turn-off stars with seismic measurements, as concluded for the Hyades (Lund et

TABLE 2
AVERAGE CLUSTER PROPERTIES.

	This work	Literature
$(m - M)_{0,sc}/mag$	9.61(3)	
$(m - M)_{0,corr}/mag$	9.57(3)	9.5-9.7 ^a
$(m - M)_{0,grid}/mag$	9.55(3)	
$M_{RGB,sc}/M_{\odot}$	1.39(2)	
$M_{RGB,corr}/M_{\odot}$	1.34(2)	1.36-1.40 ^b
$M_{RGB,grid}/M_{\odot}$	1.36(2)	
$M_{RC,sc}/M_{\odot}$	1.37(9)	
$M_{RC,corr}/M_{\odot}$	1.40(9)	1.40-1.42 ^b
$M_{RC,grid}/M_{\odot}$	1.40(3)	
Age _{grid} /Gyr	3.46(13)	3.5-4.6 ^c

^aSee review in Geller et al. (2015).

^bExtrapolated from eclipsing binary (assuming no mass loss).

^cVandenBerg & Stetson (2004); Sarajedini et al. (2009); Barnes et al. (2016); Gonzalez (2016).

al. in preparation). We summarize the results of this section in Table 2.

6. CONCLUSION

Our analysis of K2 campaign-5 data demonstrates clear detection of oscillations in the red giants of M67, and confirms previous claims of tentative detections in a few bright giants. The high quality of the K2 data enables us to measure global asteroseismic properties of stars in M67 for the first time.

From these we infer the stellar radius (hence distance), mass, and age. The distance and RGB mass are in agreement with literature values based on isochrone-fitting and the dynamical mass of a near turn-off (early subgiant) star in an eclipsing binary system. The seismic-informed age is on the lower end of independent determinations; reflecting that our seismic sample does not include turn-off stars. Our results lend support for the asteroseismic scaling relations (when corrected for well-understood offsets) as ways to obtain fundamental stellar properties. However, a more precise independent determination of stellar mass at the 0.01-0.02 M_{\odot} level, for example from eclipsing binaries, would be desirable in future to conclude which seismic approach is the most favorable. It would also be interesting to compare our results, distance in particular, with what will be obtained from Gaia.

We acknowledge Susan Agrain, Tim Bedding, Karsten Brogaard, Hans Kjeldsen, Daniel Huber, Marc Pionsonneault, and Jie Yu for fruitful discussions and helpful comments. Funding for the Stellar Astrophysics Centre is provided by The Danish National Research Foundation (Grant DNR106). The research was supported by the ASTERISK project (ASTERoseismic Investigations with SONG and Kepler) funded by the European Research Council (Grant agreement no.: 267864). D.S. acknowledges support from the Australian Research Council. A.V. is supported by the NSF Graduate Research Fellowship, Grant No. DGE 1144152. VSA acknowledges support from VILLUM FONDEN (research grant 10118).

REFERENCES

- Alam, S., et al. 2015, *ApJS*, 219, 12
 Barnes, S. A., Weingrill, J., Fritzewski, D., Strassmeier, K. G., & Platais, I. 2016, *ApJ*, 823, 16
 Basu, S., et al. 2011, *ApJ*, 729, L10
 Bessell, M. S., & Wood, P. R. 1984, *PASP*, 96, 247
 Brogaard, K., et al. 2012, *A&A*, 543, A106
 Casagrande, L., Ramírez, I., Meléndez, J., Bessell, M., & Asplund, M. 2010, *A&A*, 512, A54
 Casagrande, L., & VandenBerg, D. A. 2014, *MNRAS*, 444, 392
 Casagrande, L., et al. 2014, *ApJ*, 787, 110
 Christensen-Dalsgaard, J., Duvall, Jr., T. L., Gough, D. O., Harvey, J. W., & Rhodes, Jr., E. J. 1985, *Nature*, 315, 378
 Corsaro, E., et al. 2012, *ApJ*, 757, 190
 Dinescu, D. I., Demarque, P., Guenther, D. B., & Pinsonneault, M. H. 1995, *AJ*, 109, 2090
 Duvall, Jr., T. L., Dziembowski, W. A., Goode, P. R., Gough, D. O., Harvey, J. W., & Leibacher, J. W. 1984, *Nature*, 310, 22
 Flower, P. J. 1996, *ApJ*, 469, 355
 Geller, A. M., Latham, D. W., & Mathieu, R. D. 2015, *AJ*, 150, 97
 Gilliland, R. L., et al. 1991, *AJ*, 101, 541
 —. 1993, *AJ*, 106, 2441
 Gökay, G., Gürol, B., & Derman, E. 2013, *AJ*, 146, 123
 Gonzalez, G. 2016, *MNRAS*, 459, 1060
 Guggenberger, E., Hekker, S., Basu, S., & Bellinger, E. 2016, *MNRAS*, 460, 4277
 Hekker, S., et al. 2011, *A&A*, 530, 100
 Howell, S. B., et al. 2014, *PASP*, 126, 398
 Huber, D., Stello, D., Bedding, T. R., Chaplin, W. J., Arentoft, T., Quirion, P., & Kjeldsen, H. 2009, *Communications in Asteroseismology*, 160, 74
 Huber, D., et al. 2010, *ApJ*, 723, 1607
 —. 2016, *ApJS*, 224, 2
 Jeffries, Jr., M. W., et al. 2013, *AJ*, 146, 58
 Kallinger, T., et al. 2014, *A&A*, 570, A41
 Kjeldsen, H., & Bedding, T. R. 2011, *A&A*, 529, L8
 Mathur, S., et al. 2011, *ApJ*, 741, 119
 Miglio, A., et al. 2012, *MNRAS*, 419, 2077
 —. 2013, *MNRAS*, 429, 423
 Montgomery, K. A., Marschall, L. A., & Janes, K. A. 1993, *AJ*, 106, 181
 Mosser, B., et al. 2011, *A&A*, 525, L9
 Pace, G., Pasquini, L., & François, P. 2008, *A&A*, 489, 403
 Pietrinferni, A., Cassisi, S., Salaris, M., & Castelli, F. 2004, *ApJ*, 612, 168
 Rodríguez, E., & Breger, M. 2001, *A&A*, 366, 178
 Salaris, M., & Cassisi, S. 2005, *Evolution of Stars and Stellar Populations*, 400
 Sanders, W. L. 1977, *A&AS*, 27, 89
 Sandquist, E. L., et al. 2013, *ApJ*, 762, 58
 Sarajedini, A., Dotter, A., & Kirkpatrick, A. 2009, *ApJ*, 698, 1872
 Sharma, S., Stello, D., Bland-Hawthorn, J., Huber, D., & Bedding, T. R. 2016, *ApJ*, 822, 15
 Silva Aguirre, V., et al. 2015, *MNRAS*, 452, 2127
 Stello, D., Kjeldsen, H., Bedding, T. R., & Buzasi, D. 2006, *A&A*, 448, 709
 Stello, D., et al. 2007, *MNRAS*, 377, 584
 —. 2009, *ApJ*, 700, 1589
 —. 2010, *ApJ*, 713, L182
 —. 2011a, *ApJ*, 737, L10
 —. 2011b, *ApJ*, 739, 13
 —. 2014, *ApJ*, 788, L10
 —. 2015, *ApJ*, 809, L3
 Taylor, B. J. 2007, *AJ*, 133, 370
 VandenBerg, D. A., & Stetson, P. B. 2004, *PASP*, 116, 997
 Vanderburg, A., & Johnson, J. A. 2014, *PASP*, 126, 948
 Vanderburg, A., et al. 2016, *ApJS*, 222, 14
 White, T. R., Bedding, T. R., Stello, D., Christensen-Dalsgaard, J., Huber, D., & Kjeldsen, H. 2011, *ApJ*, 743, 161
 Yu, J., Huber, D., Bedding, T. R., Stello, D., Murphy, S. J., Xiang, M., Bi, S., & Li, T. 2016, *arXiv:1608.05803*